

Full length article

Energetics of point defects in rocksalt structure transition metal nitrides: Thermodynamic reasons for deviations from stoichiometry

Karthik Balasubramanian ^a, Sanjay V. Khare ^b, Daniel Gall ^{c,*}^a Department of Mechanical, Nuclear and Aerospace Engineering, Rensselaer Polytechnic Institute, Troy, NY, 12180, USA^b Department of Physics and Astronomy, University of Toledo, 2801 West Bancroft Street, Toledo, OH, 43606, USA^c Department of Materials Science and Engineering, Rensselaer Polytechnic Institute, Troy, NY, 12180, USA

ARTICLE INFO

Article history:

Received 4 June 2018

Received in revised form

30 July 2018

Accepted 31 July 2018

Available online 3 August 2018

Keywords:

Transition metal nitrides

Point defects

Vacancy

Interstitial

Schottky pair

ABSTRACT

First principle calculations of point defect formation energies in group 3–6 transition metal (Me) nitrides MeN_x are employed to explain the thermodynamic reasons for the large reported compositional range (typically $x = 0.7\text{--}1.3$) in the rocksalt structure. Both under-stoichiometric ($x < 1$) and over-stoichiometric ($x > 1$) compositions are due to relatively low vacancy formation energies that decrease from an average of 2.7 and 4.5 eV for nitrogen and cation vacancies in group 3 nitrides (ScN, YN, LaN) to -1.8 and -0.8 eV in group 6 nitrides (CrN, MoN, WN), indicating that they become thermodynamically stable at zero temperature for group 6 and for group 4–6 nitrides, respectively. Similarly, nitrogen and cation interstitials in tetragonal and 111- or 110-split configurations are unstable for groups 3–5 but become thermodynamically stable for group 6 nitrides, consistent with the mechanical instability of the latter compounds. All antisite defects possess high formation energies and are unlikely to form. The nitrogen chemical potential at finite temperatures and in equilibrium with a N_2 gas is strongly affected by the vapor phase entropy, leading to shifts in the defect free energy of, for example, 1.2 eV at 1 Pa N_2 at 800 K, causing an increasing likelihood for nitrogen vacancies and cation interstitials at elevated temperatures. In addition, the configurational entropy of point defects causes a correction of e.g. 0.4 eV for a 1% vacancy defect concentration at 800 K. Considering these entropy contributions leads to predicted temperature windows for stoichiometry of e.g. 200–1100 K for TiN, 500–1400 K for ZrN, and 1200–1400 K for HfN, while considerable cation and nitrogen vacancy concentrations are expected for temperatures below and above these ranges, respectively. Schottky pair defects are predicted in VN for $T > 200$ K and in NbN, TaN, and group 6 nitrides at all temperatures, independent of the N_2 partial pressure. The overall results show that thermodynamic arguments (even in the absence of kinetic barriers) can explain many of the reported composition vs temperature and pressure relationships in rocksalt structure nitrides.

© 2018 Acta Materialia Inc. Published by Elsevier Ltd. All rights reserved.

1. Introduction

Transition metal nitrides are widely used as hard [1–4] and protective [5,6] coatings and as diffusion barrier layers [3,7–14] due to their excellent thermal stability, mechanical properties, and corrosion resistance [1,3,7,8,14–18]. Stoichiometric nitrides of the early transition metals generally crystallize in the rocksalt structure, including ScN [19], TiN [20], HfN [8], ZrN [21], VN [22], NbN [23], TaN [16], CrN [24], MoN [25], WN [26], although hexagonal phases of NbN [27,28], MoN [29–31], TaN [32] and WN [33] have

also been reported, indicating that growth conditions such as temperature and pressure influence the crystal structure. In addition, most of these nitrides exhibit large single-phase fields, that is, they exhibit a rock-salt structure over a considerable composition range. For example, rock-salt TiN_x has been synthesized for x ranging from 0.67 to 1.3 [34–38], suggesting a considerable point defect concentration that results in the reported compositional variation. In fact, it is often difficult to experimentally synthesize stoichiometric transition metal nitrides, which has been attributed to these refractory nitrides having high kinetic barriers for stoichiometric nitride formation including N_2 dissociation but also exhibiting nitrogen loss at high temperature as reported for NbN [23], CrN [24], HfN [39], WN [26], TaN [16], and MoN [25], leading to

* Corresponding author.

E-mail address: galld@rpi.edu (D. Gall).

the formation of point defects. In many cases, it is unclear which point defect type is responsible for the deviation from stoichiometry, as cation and anion vacancies, interstitials, and antisite substitutions all can result in comparable composition variations and have been proposed for various transition metal nitrides [23,34,36,39–45].

Point defects cause significant changes to the structural, electrical and mechanical properties of transition metal nitrides. For example, both cation and anion vacancies in semi-conducting or semi-metallic rocksalt ScN [46,47] induce metallic conduction by acting as n- and p-type dopants. Vacancies also cause dramatic changes in mechanical properties, decreasing the elastic modulus for TiN [34,48], increasing the elastic moduli for NbN [23] and HfN [49], and stabilizing the mechanically unstable cubic structures of WN [50] and MoN [26,51]. Furthermore, vacancies contribute to stabilizing thermodynamically metastable structures such as $Ti_xW_{1-x}B_2$ [52], $Ti_{1-x}Al_xN$ [53], $Mo_{1-x}Al_xN$ [54], and MoN [25,51]. Experimental studies have reported the presence of point defects for a range of transition metal nitrides, including TiN [36,40,41,55], HfN [40,42], ZrN [40,43], NbN [23,28], TaN [45,56] and CrN [44,57], suggesting the presence of cation/anion vacancies and anion interstitials in these nitrides. In addition, some computational studies have explored the energetics of point defects in group 4–6 nitrides and found that anion vacancies are thermodynamically unfavorable for TiN [58], ZrN [58], HfN [42,58], and magnetic CrN [59], but are stable for MoN [60], TaN [60,61], and WN [50], while cation vacancies are thermodynamically stable for all the above mentioned nitrides. Anion interstitials, meanwhile, are found to be thermodynamically stable for MoN [60], and TaN [60,61]. However, a comprehensive study of the various point defects in the transition metal nitrides of group 3–6 and a resulting prediction of the likely point defect for each nitride is still missing. In short, point defects considerably affect the physical properties of transition metal nitrides. However, there is no established knowledge regarding which point defects are most likely to form for specific nitrides. This motivates our study focusing on the point-defect energetics of all transition metal nitrides that most commonly crystallize in the rocksalt structure.

In this paper, we calculate the formation energies for cation and nitrogen vacancies, interstitials, and antisite defects using first principle methods. We find that anion and cation vacancies are the lowest energy defects, with formation energies decreasing with increasing group and row and becoming negative (indicating thermodynamic stability) for cation vacancies in group 4–6 and for nitrogen vacancies in group 6 nitrides. Antisite defects in all nitrides and cation interstitials in group 3–5 nitrides have high formation energies and are therefore unlikely to form. Finite temperature effects are primarily due to the configurational entropy and the entropy of the N_2 gas that the nitride is in equilibrium with. Both entropy terms cause a reduction in the overall defect energy with increasing temperature for those point defects which cause nitrogen deficiency such as nitrogen vacancies and cation interstitials. In contrast, the two dominating entropy contributions are competing for the case of defects which cause excess nitrogen content including cation vacancies and nitrogen interstitials. As a result, many nitrides exhibit a temperature range over which an approximately stoichiometric composition is thermodynamically stable, while a considerable cation and nitrogen vacancy concentration is expected at low and high temperatures, respectively.

2. Computational procedure

First principle calculations are performed with the Vienna *ab initio* simulation package (VASP) using a plane wave basis set, periodic boundary conditions, the Perdew-Burke-Ernzerhof

generalized gradient approximation exchange correlation functional [62], and the projector-augmented wave method [63]. Computational parameters were chosen such that the total cohesive energy of 64-atom supercells is converged to within 0.1 eV, corresponding to approximately 1 meV/atom. This included a 500 eV energy cut off for the plane wave basis set and a Γ -centered $6 \times 6 \times 6$ k -point mesh. All calculations were done with cubic 64-atom $2a \times 2a \times 2a$ supercells where a is the lattice constant of the conventional 8-atom unit cell of the rock-salt structure. Convergence with respect to the super cell size was explored with larger 128-atom supercells with lattice vectors along $\langle 111 \rangle$ type directions that are $2\sqrt{3} a$ long. This leads to calculated formation energies for, for example, a nitrogen vacancy, a tetrahedral nitrogen interstitial, and a nitrogen antisite defect in TiN that deviate by 0.021, 0.007, and 0.073 eV, respectively, from the result using the 64-atom supercell, indicating a defect-energy convergence for TiN <0.1 eV. We assume the uncertainty to be approximately translatable to the other nitrides, such that all reported defect energies are expected to have an accuracy of ~ 0.1 eV.

The total energy E_{config} of defect-containing supercells is calculated by allowing atomic positions and the unit cell volume to relax until the energy is converged to 10^{-4} eV while constraining the cell to retain cubic symmetry even if the symmetry of the point defect does not exhibit cubic symmetry. In our study, the only defects which break the cubic symmetry are split interstitials. Test calculations of split interstitials in TiN indicate that the energy reduction due to cell shape relaxation is only 0.04 eV, which is below our overall computational accuracy of 0.1 eV. Thus, the type of unit cell relaxation has a negligible effect on the presented formation energies. In addition, the approach of constraining the supercell to remain cubic corresponds to the expected overall average cubic structure of a crystal with randomly orientated point defects, as expected for experimental nitride growth.

The formation energy E_f of a point defect is determined using

$$E_f = E_{\text{config}} - n_{\text{Me}} \mu_{\text{Me}} - n_{\text{N}} \mu_{\text{N}}, \quad (1)$$

where E_{config} is the total energy calculated for a particular relaxed configuration, μ_{Me} and μ_{N} are the chemical potentials of the transition metal and nitrogen, and n_{Me} and n_{N} are the number of transition metal and nitrogen atoms in the supercell, respectively. The chemical potential of nitrogen at zero temperature $\mu_{\text{N}}^0 = -8.317$ eV is the zero-temperature formation energy of a single nitrogen atom in a nitrogen molecule which is obtained by calculating the energy of a nitrogen molecule in a $15 \times 15 \times 15 \text{ \AA}^3$ cube. The zero-temperature chemical potential of the transition metal is determined from $\mu_{\text{Me}}^0 = E_{\text{MeN}}/32 - \mu_{\text{N}}^0$, where E_{MeN} is the calculated energy of a defect-free 64-atom super cell. That is, we calculate the formation energy of defects using as standard states molecular nitrogen and rock-salt structure stoichiometric transition metal nitride. Finite temperature and pressure effects due to volume changes are negligible, but affect the configurational entropy and the chemical potentials due to the entropy of the N_2 gas, as discussed in more detail in Section 4.

As an alternative to using the stoichiometric nitride and N_2 gas as standard states, the defect formation energies can also be calculated with respect to the transition metal in its pure metallic ground state. For this purpose, the energy of the metal is calculated using a 2-atom hcp-structure unit cell for group 4 metals and a 2-atom bcc structure for group 5 and 6 metals. These calculations are done with the same 500 eV energy cut-off as used for the nitride calculations, however, with a larger $16 \times 16 \times 16$ k -point mesh because of the larger Brillouin zone. The lattice constant of the reference metals is obtained by fully relaxing the unit cell shape and volume until an energy convergence of 10^{-4} eV is achieved.

Then, the zero-temperature chemical potential μ_{Me}^0 of the metal atom is set equal to the calculated cohesive energy per atom, and used to calculate the formation energy of a defect. Clearly, the value for μ_{Me}^0 here is different from above (where $\mu_{\text{Me}}^0 = E_{\text{MeN}}/32 - \mu_{\text{N}}^0$), which means that the choice of the standard state of the metal affects the calculated point-defect formation energies. We note that both approaches to define μ_{Me}^0 have merit. More specifically, (i) defining energies using the metal in its ground state is the most common approach in thermodynamics, while (ii) the common experimental synthesis of transition metal nitride layers by reactive sputter deposition or related methods occurs in a nitrogen gas or mixed nitrogen-argon atmosphere that guarantees that the flux of N_2 molecules impinging on the growing layer surface is typically 2–4 orders of magnitudes larger than the metal atom flux. Correspondingly, nitrogen exists both within the nitride and in its gaseous (N_2) state while metal atoms always form nitride (in the rock-salt structure) without any pockets of metal in its native crystal structure, suggesting that choosing the metal nitride and N_2 gas as standard states for all point defect configurations is most relevant from an experimental perspective. Hence, in Section 3 both pairs of standard states are used to present the calculated energies, while the subsequent Discussion Section 4 uses (for the purpose of clarity and applicability) only the metal nitride and N_2 gas as the standard states. More specifically, we present all calculated formation energies using stoichiometric nitride and N_2 gas as reference states. In addition, for defects where $n_{\text{N}} > n_{\text{Me}}$, we also present values for E_f where μ_{Me}^0 is determined from the metallic reference state and correspondingly $\mu_{\text{N}}^0 = E_{\text{MeN}}/32 - \mu_{\text{Me}}^0$.

Ten different point-defect types are investigated for each of twelve transition metal nitrides, including cation and anion vacancies, cation and anion antisite substitutions, and cation and anion interstitials with different symmetry. A cation or anion vacancy corresponds to one missing metal or nitrogen atom in the 64-atom unit cell, resulting in compositions of $\text{Me}_{31}\text{N}_{32}$ or $\text{Me}_{32}\text{N}_{31}$, respectively, where Me stands for the transition metal atoms. Cation or anion antisite defects are formed by a metal or nitrogen atom replacing an atom of the opposite type, leading to compositions of $\text{Me}_{33}\text{N}_{31}$ or $\text{Me}_{31}\text{N}_{33}$, respectively. Correspondingly, interstitial defects have compositions of $\text{Me}_{33}\text{N}_{32}$ or $\text{Me}_{32}\text{N}_{33}$. Both tetrahedral interstitial and split interstitial symmetries are explored: Tetrahedral interstitials occupy sites with a fractional position (1/8, 1/8, 1/8) in the cubic 64-atom supercell and have four cation and four anion nearest neighbors. Split interstitials are formed by two atoms of the same type occupying a single lattice site. For example, a split₁₁₀ nitrogen interstitial corresponds to a configuration where two nitrogen atoms are positioned such that the center of mass of the two atoms lies on an anion lattice position and the unit vector connecting the two nitrogen atoms is oriented along the $\langle 110 \rangle$ direction. Split interstitials with $\langle 111 \rangle$ and $\langle 100 \rangle$ orientations are also explored, but the split₁₀₀ interstitials have considerably higher formation energies and are omitted in the following Results Section 3 that presents split₁₁₀, split₁₁₁, and tetrahedral interstitials. The effect of temperature on the entropy of the N_2 gas is calculated using the Sackur-Tetrode equation [64] which calculates the entropy of an ideal gas using contributions from translational, rotational and vibrational degrees of freedom from statistical thermodynamics. The characteristic temperatures for rotational and vibrational degrees of freedom of N_2 molecules used in these entropy calculations are 2.86 and 3340 K, respectively.

3. Results

Fig. 1 is a plot of the calculated zero-temperature formation energy E_f of vacancy defects in nitrides of group 3–6 transition metals, which are also summarized in Table 1. The solid circles and

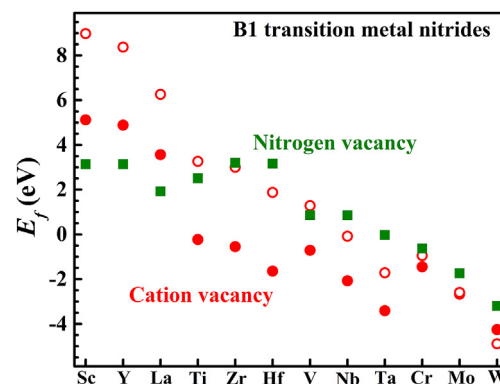


Fig. 1. Formation energy E_f of cation and anion vacancies in Group 3–6 transition metal nitrides at 0 K. Open and closed symbols are for different reference states of the metal ion, namely bulk metal or stoichiometric B1 nitride, respectively.

squares indicate E_f of cation and nitrogen vacancies with the zero-energy reference states being molecular nitrogen and defect-free rock-salt structure nitride, while the open circles show E_f for the cation vacancies when using the native elemental metal ground state as metal reference state, e.g. Ti in its hcp structure, as described in detail in Section II. The open circles have values that are $\Delta\mu_{\text{MS}}^0$ higher than the closed circles, where $\Delta\mu_{\text{MS}}^0$ is the chemical potential difference of the metal atom between the standard states, as also listed in Table 1, which corresponds to the negative of the energy for formation of rock-salt nitride from elemental metal and molecular nitrogen.

ScN has cation and anion vacancy formation energies of 5.1 and 3.1 eV. These values decrease when moving down in the group to YN with $E_f = 4.9$ and 3.1 eV and LaN with $E_f = 3.6$ and 1.9 eV. The positive values indicate that both cation and nitrogen vacancies are energetically unfavorable for group 3 nitrides. The nitrogen vacancy formation energies of group 4 nitrides have similar positive values, with $E_f = 2.5$, 3.2, and 3.2 eV for TiN, ZrN, and HfN, which are in good agreement with previously reported computational results indicating 2.41 eV [58,65] for TiN, 3.15 eV [58] and 3.22 eV [66] for ZrN, and 3.51 eV [58] and 3.12 eV [42] for HfN. On the contrary, the cation vacancy formation energies are negative, -0.2 , -0.5 , and -1.6 eV for TiN, ZrN, and HfN, respectively, indicating thermodynamic stability for metal vacancies in these nitrides. We note that the energies become positive, when correcting for entropy effects at finite temperatures, as discussed in Section IV. Also, using metal as reference state leads to positive $E_f = 3.3$, 3.0, and 1.9 eV for TiN, ZrN, and HfN, indicating thermodynamic stability against dissociation of stoichiometric nitrides into nitrogen-rich (cation vacancy containing) nitrides and pure metal. These latter values are in good agreement with the previously reported 3.28 eV [65] for TiN, 2.91 eV [66] for ZrN and 1.87 eV [42] for HfN.

The vacancy formation energies decrease further when moving to the right in the periodic table to group 5 nitrides, with $E_f = -0.7$, -2.1 , and -3.4 eV for metal vacancies in VN, NbN, and TaN, and $E_f = 0.9$, 0.9, and 0.0 eV for the corresponding nitrogen vacancies. The latter is in agreement with previously reported 0.1 eV for the formation of a nitrogen vacancy in TaN [61]. These low and negative values indicate an increasing thermodynamic driving force for vacancy formation in rock-salt structure group 5 nitrides. The formation energy for cation vacancies is low, even if using the V, Nb, and Ta metal as reference states, yielding $E_f = 1.3$, -0.1 , and -1.7 eV. The latter value is in good agreement with the reported -1.8 eV for cation vacancies in TaN [60,61]. For group 6, all calculated vacancy formation energies are negative, ranging from -0.6 eV for an anion vacancy in CrN to -4.9 eV for a cation

Table 1
Zero-temperature formation energies of point-defects in rocksalt-structure transition metal nitrides in units of eV per defect. T , S_{111} , and S_{110} refer to interstitials in a tetragonal or $\langle 111 \rangle$ or $\langle 110 \rangle$ oriented split configuration. $\Delta\mu_{\text{MS}}^0$ indicates the difference in the chemical potential between the metal and the N_2 reference states.

Phase	Cation vacancy	Nitrogen vacancy	Cation antisite	Nitrogen antisite	Nitrogen interstitial			Cation interstitial			$\Delta\mu_{\text{MS}}^0$
					T	S_{111}	S_{110}	T	S_{111}	S_{110}	
ScN	5.1	3.1	15.7	9.0	7.0	3.9	3.9	9.4	11.0	11.8	3.9
YN	4.9	3.1	15.4	9.0	5.9	2.8	2.6	9.5	12.0	10.9	3.5
LaN	3.6	1.9	8.4	7.8	3.8	1.0	0.8	5.2	7.2	5.6	7.5
TiN	-0.2	2.5	14.7	8.1	4.9	6.2	4.4	11.2	11.7	12.2	3.5
ZrN	-0.5	3.2	17.3	7.2	2.7	4.5	3.6	14.7	14.1	15.3	3.5
HfN	-1.6	3.2	18.9	6.3	2.6	4.4	3.7	16.3	15.6	17.1	3.5
VN	-0.7	0.9	9.5	7.1	4.3	3.9	3.1	5.7	6.0	7.7	2.0
NbN	-2.1	0.9	12.4	6.4	0.9	1.5	1.6	9.1	6.7	10.9	2.0
TaN	-3.4	0	13.7	5.6	-0.8	-0.1	0.3	10.0	6.0	11.5	1.7
CrN	-1.4	-0.6	5.3	6.7	-1.3	-4.3	-1.8	-2.9	-1.1	2.1	0.5
MoN	-2.7	-1.7	6.5	4.5	-6.0	-8.0	-9.0	-4.2	-4.1	0	0.1
WN	-4.3	-3.2	7.2	2.9	-11.0	-14.9	-13.2	-7.7	-7.6	-2.9	-0.6

vacancy in WN, indicating a strong thermodynamic driving force for vacancy formation in group 6 nitrides. We note that, for consistency purposes, all calculations are done for stoichiometric non-magnetic cubic rock-salt structure nitrides, despite that their ground state may be a different phase. More specifically, the reported zero-temperature ground state for CrN is antiferromagnetic and has a 1.7° distorted structure with a magnetic moment of $2.4 \mu_{\text{B}}$ [67–69]. We calculate for CrN in the antiferromagnetic phase vacancy formation energies of 1.8 and 1.6 eV for cation and anion vacancies, respectively, in reasonable agreement with the reported 2.28 eV [59] for nitrogen vacancies. Similarly, MoN is most stable in a monoclinic phase [51], and the reported ground state for WN is a NbO phase [15,50,70]. The fact that the rock-salt phase of these three nitrides is thermodynamically unstable is consistent with both anion and cation vacancies having negative formation energies. This is because the latter indicates that the energy of the rock-salt phase can be reduced without changing its composition by the introduction of vacancies, which effectively means that lower-energy phases exist.

The overall data in Fig. 1 indicates an increasing preference for the formation of both cation and anion vacancies when moving both down the group and along the period for nitrides of metals from groups 3–6. This suggests a decreasing stability of nitrides in the rocksalt structure with increasing group, that is when moving to the right in the periodic table. We attribute the decreasing stability to the filling of overlapping metal d - t_{2g} orbitals, which increase the importance of cation-cation bonds, therefore favoring structures with a reduced distance between neighboring metal ions. Conversely, the introduction of cation and/or anion vacancies reduces the number of electrons and therefore the filling of metal d - t_{2g} orbitals, stabilizing the rocksalt structure. Similar arguments have previously been used to explain the mechanical stability/instability of transition metal nitrides [71–73]. Particularly, the defect-free rocksalt phase of group 6 nitrides (for which both the anion and cation vacancies are thermodynamically favorable) is mechanically unstable due to overlapping d - t_{2g} orbitals which result in negative shear moduli [26,50,51,67,70,74,75]. We note that the magnetic character of CrN plays an important role in mechanically stabilizing the rocksalt structure, with a reported negative and positive shear modulus for paramagnetic and antiferromagnetic rocksalt-structure CrN, respectively [74,75]. The vacancy formation energy also decreases while moving down the group. We attribute this to the increasing overlap of d - t_{2g} orbitals associated with the increased screening when moving down in the periodic table. Correspondingly, moving down favors a reduced electron density in metal d -orbitals, which is facilitated by the introduction of vacancies.

A Schottky pair is a defect structure consisting of an anion and a cation vacancy. Its formation or annihilation does not affect the overall composition, that is, Schottky defects can form within nitrides without the need to adsorb or release nitrogen from/to the vapor phase. Correspondingly, their formation energies are unaffected by the chemical potentials μ_{Me} and μ_{N} which are dependent on the reference state, particularly the chosen metal phase and the entropic effects in the N_2 gas, as discussed in Sections II and IV, respectively. Therefore, Schottky defects are unaffected by external parameters and represent a valuable discussion point. Here we determine their formation energy from the sum of the calculated E_f values for cation and nitrogen vacancies, neglecting the interaction energy between opposite vacancy defects. The formation energy for Schottky pairs decreases with increasing group number, similar to individual vacancies. It is positive for all group 4 nitrides but becomes negative, indicating thermodynamic favorability, for NbN and TaN with $E_f = -1.2$ and -3.4 eV, respectively. This is supported by experimental reports which suggest vacancies of both types being present in these nitrides [16,23,28,56]. Schottky vacancy pairs are even more stable for group 6 nitrides, with $E_f = -2.1$, -4.4 and -7.5 eV for non-magnetic CrN, MoN and WN, respectively. This is again supported by experimental observations of cation and nitrogen vacancies in MoN and WN [25,26,76]. CrN, as mentioned previously, exhibits magnetic ordering which stabilizes the structure and increases the vacancy formation energies.

Fig. 2 is a plot of the antisite defect formation energies for the same twelve rocksalt-structure transition metal nitrides. A cation antisite refers to a point defect where a metal atom replaces a nitrogen atom on an anion site, leading to a metal-rich nitride

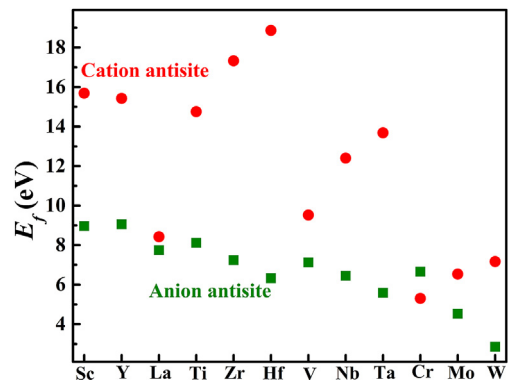


Fig. 2. Formation energy E_f of cation and anion antisite defects in rocksalt structure transition metal nitrides at zero temperature.

composition. Correspondingly, the anion antisite defect exhibits a substitutional nitrogen atom on a cation site, resulting in a nitrogen-rich compound. All plotted values use molecular nitrogen and stoichiometric nitride as reference states. The corresponding values with metal as reference state can be obtained by correcting E_f by $\Delta\mu_{\text{MS}}^0$, which is listed in Table 1. For example, the cation antisite defect formation energy for ScN of 15.7 eV (plotted in Fig. 2 and also listed in Table 1) is corrected by subtracting two times $\Delta\mu_{\text{MS}}^0$ for ScN, leading to 7.9 eV for the case where Sc metal is the reference state. The factor two is due to the Sc antisite defect resulting in two more Sc than N atoms. The plotted data indicates a general trend of a decreasing defect formation energy when moving towards the right in the periodic table, with E_f for the anion antisite defect decreasing from 9.0 eV for ScN to 2.9 eV for WN, while E_f for the cation antisite defects range from 5.3 to 18.9 eV. These large formation energies indicate a strong thermodynamic driving force for the annihilation of antisite defects. Correspondingly, we envision that antisite defects can only form under kinetically limited synthesis conditions that involve energetic particles as in ion-beam deposition methods or plasma processing including sputter deposition.

Fig. 3(a) shows the formation energy for nitrogen interstitials in rock-salt structure transition metal nitrides. The plot includes three configurations, split₁₁₀, split₁₁₁ and tetrahedral, as described in Section II. The nitrogen interstitial with the lowest energy configuration for group 3 nitrides is the split₁₁₀ configuration, with $E_f = 3.9, 2.6,$ and 0.8 eV for ScN, YN, and LaN, respectively. The formation energy of the split₁₁₁ is just 0–0.3 eV higher, and for the case of ScN is degenerate (within the 0.1 eV accuracy) with the split₁₁₀. Conversely, E_f for the tetrahedral configurations are 3.0–3.3 eV higher, rendering their formation very unlikely. The preference for the split configurations may be associated with the relatively large lattice constant of group 3 nitrides, providing sufficient space for nitrogen dumbbells in either a split₁₁₀ or

split₁₁₁ orientation. In contrast, for nitrides of group 4 and 5 transition metals (Ti through Ta), the tetrahedral nitrogen interstitial has a similar formation energy as the competing configurations, and is in fact the lowest-energy interstitial configuration for ZrN, HfN, NbN, and TaN, while the first-row transition metal nitrides TiN and NbN prefer the split₁₁₀ configuration. The preference for the more symmetric tetrahedral configuration may be the smaller induced strain in combination with increasing non-directional metallic bonding that is facilitated by weaker screening and a higher valence electron concentration when moving down and to the right in the periodic table, respectively. We note, however, that the larger entropy of the split interstitials may favor them over the tetrahedral configurations at finite temperatures, as discussed in Section IV. The calculated formation energies agree well with previous studies. For example, $E_f = 4.4$ eV for the split₁₁₀ vacancy in TiN is in good agreement with the reported 4.60 eV [58] and 4.33 eV [65]. Similarly, $E_f = 2.7$ and 2.6 eV for the tetrahedral N interstitial in ZrN and HfN is in good agreement with the reported 2.7 eV [66] for ZrN and 2.66 eV [42] for HfN. The plotted E_f values decrease steeply when moving down in column 5, from 3.1 eV for VN to 0.9 and -0.8 eV for NbN and TaN. This trend indicates a decreasing stability of the rock-salt structure, consistent with previous studies which report the competing hexagonal phase of TaN to be the most stable at the 1:1 composition [56,77,78], and dynamic instability of all three group 5 transition metal nitrides [75,79–81]. Similarly, and even more pronounced, the plotted E_f for group 6 decreases from -4.3 for CrN to -8.0 eV for MoN to -14.9 eV for WN. These negative values are consistent with the reported thermodynamic instability of the rock-salt structure for group 6 nitrides [25,50,51,74,79].

Fig. 3(b) is a plot of the corresponding cation interstitial formation energies. All nitrides of transition metals from groups 3–5 (ScN through TaN) exhibit cation interstitial E_f values that are larger than 5 eV, which renders them unlikely to form. The formation energies remain positive (with the exception of LaN) even when choosing the alternative metallic reference state to define the cation chemical potential, done by subtracting $\Delta\mu_{\text{MS}}^0$ from the plotted E_f values. For example, $E_f = 11.2, 14.1,$ and 15.6 eV for TiN, ZrN, and HfN reduces to 7.7, 10.6 and 12.8 eV, respectively, when using metallic reference states. These values are in reasonable agreement with the previously reported 8.28 eV [65] for TiN, 10.41 eV [66] for ZrN and 11.01 eV [42] for HfN. The positive E_f values for metal interstitials indicate that there is a thermodynamic driving force for segregation of cation interstitials to form metallic precipitates. In contrast, group 6 transition metal nitrides exhibit negative cation interstitial formation energies of $-2.9, -4.2,$ and -7.7 eV for their lowest-energy tetrahedral configurations in CrN, MoN, and WN, respectively. These relatively large negative values are attributed to the rocksalt phase not being the lowest energy structure for these nitrides, such that the interstitial metal atoms nucleate a structural relaxation that lowers the overall energy. We note here that both cubic MoN [25,51,82] and cubic WN [26,50] are more stable in the NbO phase than in the rocksalt phase. The NbO phase can be described as a rocksalt structure containing vacancies on 25% of both cation and anion sites. Correspondingly, one would expect vacancies in MoN and WN to be more stable than interstitials, opposite to the results presented here and listed in Table 1. We attribute this difference to (i) the NbO phase exhibiting a (low energy) dense ordered vacancy array while our calculations (in contrast) determine formation energies of isolated vacancies and (ii) the atomic relaxations for these mechanically unstable MoN and WN rocksalt phases are stronger for supercell calculations containing interstitials (which cause compressive strain) than vacancies which cause tensile strain and tend to stabilize the rock-salt phase [25,50].

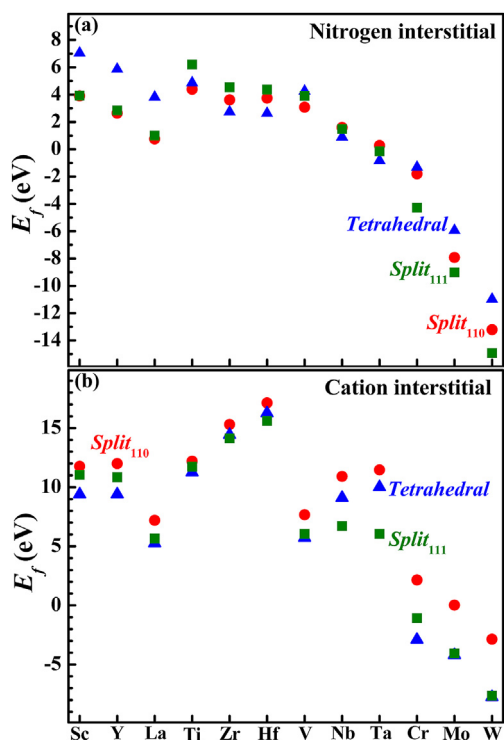


Fig. 3. Formation energy E_f of (a) anion interstitials and (b) cation interstitials in rock-salt structure group 3–6 transition metal nitrides at 0 K.

4. Discussion

This discussion section is divided into two parts: We first discuss finite temperature effects by estimating the configurational entropy contributions and changes in the chemical potential of the N_2 gas during nitride synthesis, leading to shifts in the defect formation energies from the zero-temperature results presented in the previous section. Secondly, we discuss which point defects are most likely to account for deviations from a stoichiometric 1:1 metal-to-nitrogen ratio in rock-salt structure transition metal nitrides.

4.1. Finite temperature effects

Thin film deposition of transition metal nitrides is done at various temperatures, typically within the range $T = 300\text{--}1200$ K. In contrast, all calculations in this manuscript are done at zero temperature and, correspondingly, all formation energies presented in Section 3 are $T = 0$ K values. Here we discuss how temperature may affect the presented E_f values in order to more appropriately apply the results to thin film synthesis. The thermodynamics of the point defect formation energy is affected by the temperature in various aspects. However, many of them can be neglected within the accuracy of 0.1 eV of the present study. For example, temperature causes an increase in the lattice constant and a corresponding increase in the average bond length which directly reduces the defect formation energy, however, by a negligible amount of <0.01 eV, as estimated using $C_p = C_v + VT_B\alpha^2$ and $\Delta H = C_p \Delta T$, where C_p and C_v are the heat capacities at constant pressure and volume, B is the bulk modulus, α is the volumetric thermal expansion coefficient and ΔH is the change in formation energy due to change in temperature. Also, the mechanical work performed during expansion of the nitride due to either temperature or the introduction of a point defect is very small, $<10^{-6}$ eV per atom or defect at atmospheric pressure and $<10^{-11}$ eV at a typical vapor deposition pressure of 1 Pa (7 mTorr).

In contrast, the configurational entropy due to the introduction of defects contributes significantly to the overall free energy and thus the free energy for defect formation. The contribution due to the configurational entropy associated with the random distribution of point defects is determined from statistical thermodynamics using a combinatorial approach which yields for vacancies $TS_{\text{config}} = -k_B T [\ln \xi + ((1-\xi)/\xi) \ln(1-\xi)]$, where S_{config} is the entropy per defect, ξ is the defect concentration in units of number of defects per cation site, and k_B is the Boltzmann constant. The configurational entropy of antisites is determined with the same expression as that of vacancies, while the configurational entropy of Schottky defects is twice that of vacancies. For interstitials, $TS_{\text{config}} = -k_B T [\ln \lambda \xi + (1-\lambda \xi) \ln(1-\lambda \xi)/\lambda \xi]$, where $\lambda = 1/6, 1/4$ and $1/2$, for split₁₁₀, split₁₁₁ and tetrahedral configurations, respectively, because there are six $\langle 110 \rangle$ and four $\langle 111 \rangle$ directions for the orientational alignment of the split interstitial, and there are two tetrahedral sites per cation lattice site in the rocksalt structure.

Fig. 4(a) shows the contributions from the different defect types to the configurational entropy. It is plotted as $-TS_{\text{config}}$ vs temperature, indicating by how much the configurational entropy reduces the free energy per defect. The solid green line is for a $\xi = 1\%$ concentration of vacancies. It increases from 0 eV at 0 K to 0.2, 0.5 and 1.0 eV at 500, 1000, 2000 K, illustrating the decreasing free energy for vacancy formation with increasing temperature. This energy correction is more pronounced at small defect concentrations, as indicated by the dashed and dash-dotted lines for $\xi = 0.1\%$ and 10%, respectively, with the largest plotted correction of 1.4 eV for $\xi = 0.1\%$ at 2000 K. Fig. 4(a) also shows the contribution to the free energy from the configurational entropy for a Schottky defect with a concentration of 1%, which corresponds to 1% of cation and

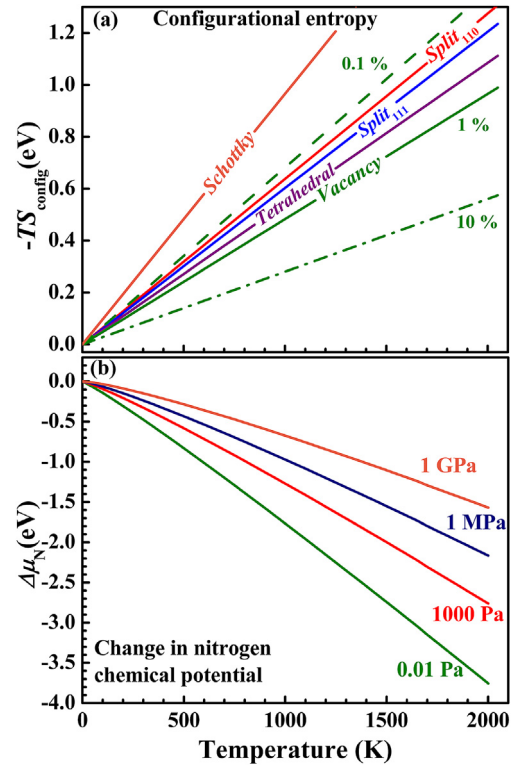


Fig. 4. Finite temperature corrections: (a) the configurational entropy S_{config} contribution plotted as $-TS_{\text{config}}$ vs temperature T , for vacancies with concentrations of $\xi = 0.1\%$, 1%, and 10%, and for Schottky pairs and tetrahedral, split₁₁₀ and split₁₁₁ interstitials with $\xi = 1\%$. (b) Correction in the chemical potential $\Delta\mu_N$ of nitrogen as a function of temperature and partial pressure of the N_2 gas.

1% of anion sites being vacant. It is twice that of a vacancy defect and is therefore 0.5, 1.0, and 1.9 eV at 500, 1000, and 2000 K, respectively. The configurational entropy for the interstitial defects is also larger than for the vacancies, because of the larger number of possible configurations. More specifically, $-TS_{\text{config}}$ of tetrahedral, split₁₁₁, and split₁₁₀ interstitials is larger than for the vacancy defects by approximately $k_B T \ln(2)$, $k_B T \ln(4)$, and $k_B T \ln(6)$, corresponding to a total $-TS_{\text{config}}$ at 2000 K of 1.1, 1.2, and 1.3 eV, respectively.

The vibrational free energy including the zero point vibrational energy and the contribution from the vibrational entropy TS_{vib} also contribute to the free energy of point defects in transition metal nitrides. For example, using a characteristic frequency of 10^{13} s^{-1} for a high-energy acoustic or a low-energy optical mode of a typical nitride [75,79,83,84], the entropy contribution from a single oscillator is $TS_{\text{vib}} = 0.09, 0.3$, or 1.1 eV at 500, 1000, or 2000 K, suggesting that vibrational contributions can be considerable. However, previous detailed studies employing complete vibrational spectra indicate much smaller average contributions [85], reporting, for example, a vibrational free energy per atom in CrN of 0.08, 0.02, and -0.15 eV at 0, 500, and 1000 K, respectively [85]. These values are comparable to the energy accuracy of 0.1 eV in our study, suggesting that these contributions can be neglected. In addition, the vibrational contribution to the defect formation energy is the difference between the vibrational free energies of the defect containing configuration and the atoms in their reference states, such that the contribution to the defect free energy may be considerably smaller than the vibrational free energy per atom in the nitride. Therefore, in this study, we neglect the vibrational contributions to the point defect free energies. We also note that correct accounting of these contributions would require the determination of the

temperature-dependent phonon density of states, which is well beyond the scope of this study.

The largest temperature effect to the free energy for defect formation is due to the entropy in the nitrogen gas, which is used as the reference state to determine μ_N . The N_2 gas exhibits translational, rotational and vibrational degrees of freedom, where particularly the translational degrees of freedom contribute substantially to the nitrogen chemical potential μ_N . Fig. 4(b) shows a plot of the change in the chemical potential of nitrogen $\Delta\mu_N$ as a function of temperature and pressure. It is calculated using the Sackur-Tetrode [64] equation as mentioned in the procedure section, using characteristic temperatures for rotational and vibrational degrees of freedom of N_2 molecules of 2.86 and 3340 K [86]. With increasing temperature, the chemical potential of nitrogen decreases nearly linearly. For example, at a pressure of 0.01 Pa, $\Delta\mu_N$ decreases from 0 eV at 0 K to -0.8 eV at 500 K and to $\Delta\mu_N = -1.8$ and -3.7 eV at 1000 and 2000 K, respectively. This effect is less pronounced at higher pressures with, for example, $\Delta\mu_N = 0, -0.7, -1.6$ and -3.4 eV at 1 Pa and $\Delta\mu_N = 0, -0.4, -1.0$ and -2.1 eV at 1 MPa at 0, 500, 1000, and 2000 K. A decrease in the chemical potential of nitrogen results also in a corresponding increase in the chemical potential of the metal ion. This is because we use the stoichiometric nitride as standard state for the cation, as discussed in Section II. The corrected chemical potentials of the anions and cations therefore become:

$$\mu_N = \mu_N^0 + \Delta\mu_N \quad (2a)$$

$$\mu_{Me} = \mu_{Me}^0 - \Delta\mu_N \quad (2b)$$

Based on these equations, the sum $\mu_N + \mu_{Me} = \mu_N^0 + \mu_{Me}^0$ is independent of $\Delta\mu_N$. Therefore, the energetics of defects which retain the N/Me ratio like Schottky defects are unaffected by changes in the nitrogen chemical potential such that their temperature dependences are only due to contributions by the configurational entropy discussed above. In contrast, the formation energy of defects for which $n_N < n_{Me}$, including N vacancies, cation interstitials, and cation antisite defects is reduced at elevated temperatures by the decreasing $\Delta\mu_N$, making these defects thermodynamically more favorable. Thus, a N vacancy, for example, becomes more stable as the temperature is increased because the N atom has an increasing preference to move into the N_2 gas which has a considerably higher entropy than the solid transition metal nitride. In addition, the favorability of these defects is enhanced by contributions from the configurational entropy, as discussed above. Conversely, point defects which result in $n_N > n_{Me}$ exhibit formation energies which increase with increasing temperature due to the decreasing $\Delta\mu_N$. Correspondingly, these defects including cation vacancies, nitrogen interstitials and nitrogen antisite defects become thermodynamically less favorable with increasing T . This effect is partially compensated by the contribution from the configurational entropy which lowers the free energy of any type of point defect. We note that, in principle, the configurational entropy can more than compensate the decrease in $\Delta\mu_N$, such that nitrogen rich point defects could also increase their thermodynamic stability with increasing T . However, as evident from Fig. 4, the magnitude of $\Delta\mu_N$ is generally larger than of TS_{config} , and therefore an increasing temperature reduces the free energy of nitrogen rich point defects only for very small defect concentrations of less than $\sim 10^{-5}$ at e.g. 1 Pa.

For example, the formation energy for a Ti vacancy in TiN at zero temperature is -0.2 eV, as listed in Table 1. However, increasing the temperature at $p_{N_2} = 0.01$ Pa and at a defect concentration of 1% leads to free energies of 0.4 and 1.1 eV at 500 and 1000 K, respectively. At higher pressure, this energy increase is less pronounced,

with for example 0.3 and 0.8 eV at 500 and 1000 K for $p_{N_2} = 1$ MPa. Nevertheless, finite temperatures move the free energy for formation of Ti vacancies from negative to positive, such that their expected concentration is well below 1% for TiN in thermodynamic equilibrium with an N_2 gas. We note that the range of realistic N_2 partial pressures during reactive sputter deposition is limited to approximately 10^{-3} to 10 Pa. In contrast, high-pressure synthesis methods using diamond anvil cells have been employed to achieve N_2 pressures in excess of 30 GPa [87,88]. In this context, we note that some (relatively uncommon) high strength nitrides such as OsN_2 [87], IrN_2 [87], Re_2N and Re_3N [88], Ta_2N_3 [89], W_2N_3 and W_3N_4 [90] have been reported to form at high pressures and temperatures but are unstable at lower pressures. We attribute the need for high temperatures to kinetic barriers that need to be overcome for nitridation, while the high pressure is required such that μ_N is high and the nitride is thermodynamically favored over phase separation into N_2 gas and a pure metal or understoichiometric nitride.

4.2. Deviations from stoichiometry in rock-salt structure transition metal nitrides

Rock-salt structure transition metal nitride MeN_x layers are known to exhibit large single phase fields [26,34,39,45,51,91] with understoichiometric (i.e. nitrogen deficient/cation rich) or overstoichiometric (nitrogen rich/cation deficient) compositions. However, as discussed in Section I, it is typically unclear which point defects are responsible for these deviations from stoichiometry. Thus, here we discuss how the calculated defect formation energies presented in Section 3 and the finite temperature arguments presented in Section 4.1 provide insight into the question of the most likely point defects. A nitride with an overstoichiometric ($x > 1$) composition contains either cation vacancies, nitrogen interstitials and/or nitrogen antisite defects. Conversely, understoichiometry ($x < 1$) is the result of nitrogen vacancies, cation interstitials and cation antisites, while Schottky defects have no effect on the composition.

For group 3 transition metal nitrides (ScN, YN and LaN), overstoichiometric compositions are most likely caused by the presence of nitrogen interstitials which are thermodynamically preferred over cation vacancies and anion antisites. Based on the E_f values presented in Table 1, the average formation energy for nitrogen interstitials in these three nitrides is 2.4 eV, which is considerably smaller than 4.5 eV for the cation vacancies and 8.6 eV for nitrogen antisites. We note here that a single antisite defect has twice as much effect on the composition than a vacancy or an interstitial. For example, a nitrogen-to-metal ratio of $x = 1.1$ can be reached if there is one N interstitial for every 10 metal lattice sites. The same $x = 1.1$ is reached if there is one cation vacancy for every 11 metal lattice sites. However, the same $x = 1.1$ is also reached if there is one N antisite defect for every 21 metal sites. Therefore, since 4.5 eV for cation vacancies is approximately half of 8.6 eV for nitrogen antisites, these two defects have thermodynamically a similar probability of accounting for an overstoichiometric group 3 nitride. However, as mentioned above, the N interstitial is the preferred point defect for overstoichiometric compositions such that the argument between cation vacancies and anion antisites is of little importance.

Group 3 nitrides with an understoichiometric composition are expected to contain N vacancies, since their average formation energy of 2.7 eV is much smaller than 8.2 eV for cation interstitials and 13.2 eV for cation antisites. All point defect formation energies listed in Table 1 for Group 3 nitrides have positive values. Thus, none of these defects are expected when ScN, YN, or LaN are at thermodynamic equilibrium with N_2 gas at 0 K. This is a purely

academic statement since (a) N_2 is not in the vapor phase at 0 K, and (b) more importantly, kinetic barriers at low temperature inhibit the equilibrium to be reached. Nevertheless, the zero temperature energetics represents the starting point for discussing finite temperature effects.

Increasing temperature causes the chemical potentials for nitrogen and cations to decrease and increase, respectively, such that defects which cause understoichiometric compositions become increasingly favorable while overstoichiometric nitrides become thermodynamically less stable, as discussed in Section 4.1. Correspondingly, increasing temperature will lead to a decrease in the free energy of formation and ultimately thermodynamic stability of nitrogen vacancies, cation interstitials and cation antisite defects in Group 3 nitrides. To estimate the critical temperatures where stability is reached, we consider a nitrogen partial pressure of 1 Pa which is typical for thin film deposition of nitrides and a defect concentration of 1%. Using the expressions from Section 4.1 for the nitrogen chemical potential and the configurational entropy, we calculate the free energy for vacancy formation which decreases with increasing temperature and becomes zero at a critical temperature of 1400, 1400 and 900 K, for N vacancies in ScN, YN, and LaN, respectively. That is, above these critical temperatures, these compounds are expected to spontaneously form nitrogen vacancies by losing nitrogen to the 1 Pa N_2 gas, as also summarized in Table 2 and illustrated in Fig. 5. The critical temperatures for the other defects are considerably higher, 4000, 4000 and 2300 K for cation interstitials and 6800, 6700 and 3700 K for cation antisite defects in ScN, YN, and LaN, respectively. These latter temperatures are well above the nitride melting points and therefore have no practical significance besides illustrating that these defects are not expected to form, as discussed above. Similarly, Schottky pairs have unrealistically high critical formation temperatures of 8500, 8300 and 5700 K for ScN, YN and LaN, respectively. They do not affect the composition and, thus, their formation energy is independent of the changes in the nitrogen chemical potential and only affected by the configurational entropy. We note here that these critical temperatures (listed in Table 2 and illustrated in Fig. 5) are calculated for a 1% defect concentration and that, in principle, entropy causes point defects to become thermodynamically stable at any finite temperature for sufficiently small concentrations. More specifically, a reduction by one order of magnitude in the defect concentration reduces the free energy of formation by approximately $k_B T \ln(10)$, which is 0.1, 0.2 or 0.4 eV at a temperature of 500, 1000, or 2000 K, respectively. These are, however, relatively small corrections, indicating that the choice of a 1% defect concentration has only a limited effect on the determined critical temperatures.

Point defects in ScN, YN and LaN which cause overstoichiometric compositions, including nitrogen interstitials, cation vacancies and nitrogen antisites, remain thermodynamically

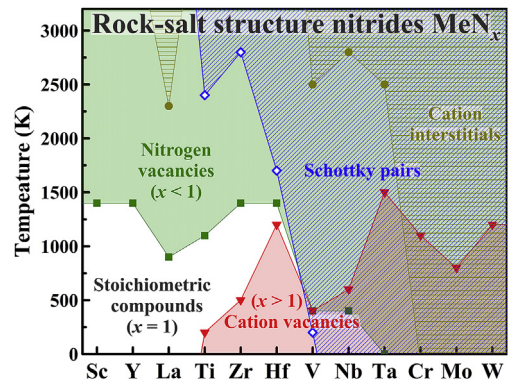


Fig. 5. The predicted temperature ranges where nitrogen vacancies, cation vacancies, Schottky pairs and cation interstitials are thermodynamically stable in rock-salt structure transition metal nitrides, for a defect concentration of 1% of cation sites and equilibrium with N_2 vapor at 1 Pa.

unstable at all temperatures. This is because the reduction in the free energy due to the configurational entropy is more than compensated by the reduction in the nitrogen chemical potential. Thus, in summary, we expect ScN, YN, and LaN to form defect free stoichiometric nitrides for $T < 1400$, 1400, and 900 K, respectively, but to become understoichiometric and contain N vacancies at higher temperatures. This is in good agreement with experimental studies which report stoichiometric ScN [19,92,93] at growth temperatures close to 1000 K. However, other experimental reports [46,94] also indicate that considerable nitrogen vacancy concentrations can be incorporated during ScN layer growth with a high Sc flux which promotes nitrogen vacancy formation due to kinetic limitations.

Group 4 nitrides, TiN, ZrN and HfN, have negative cation vacancy formation energies of -0.2 , -0.5 and -1.6 eV at 0 K. Thus, they are thermodynamically expected to form at 0 K, leading to overstoichiometric compositions. The other point defects that result in overstoichiometric compositions have positive E_f values, with an average of 7.2 and 3.2 eV for the nitrogen antisite and nitrogen interstitial, respectively. For understoichiometric TiN, ZrN and HfN, the most stable point defect is the N vacancy with $E_f = 2.5$, 2.5 and 3.2 eV, respectively, while the cation antisites and cation interstitials have considerably larger average formation energies of 17.0 and 13.6 eV, rendering them unlikely to form.

Increasing temperature increases the free energy of cation vacancies but decreases that of nitrogen vacancies. Therefore, at a N_2 partial pressure of 1 Pa, the cation vacancies that are thermodynamically stable at 0 K become unstable above critical temperatures of 200, 500, and 1200 K, for TiN, ZrN, and HfN, respectively, while N vacancies become stable above 1100, 1400, and 1400 K,

Table 2

The predicted temperature range (in K) over which point defects in rock-salt structure transition metal nitrides are thermodynamically stable in equilibrium with N_2 vapor at 1 Pa, for a defect concentration of 1% of cation sites. The symbol “-” denotes defects which are expected to be unstable at all temperatures.

Phase	Cation vacancy	Nitrogen vacancy	Schottky pair	Cation interstitial	Nitrogen interstitial
ScN	–	>1400	>8500	>4000	–
YN	–	>1400	>8300	>4000	–
LaN	–	>900	>5700	>2300	–
TiN	<200	>1100	>2400	>4700	–
ZrN	<500	>1400	>2800	>5700	–
HfN	<1200	>1400	>1700	>6100	–
VN	<400	>400	>200	>2500	–
NbN	<600	>400	>0	>2800	–
TaN	<1500	>0	>0	>2500	>0
CrN	<1100	>0	>0	>0	>0
MoN	<800	>0	>0	>0	>0
WN	<1200	>0	>0	>0	>0

respectively. Correspondingly, we expect defect-free TiN to be thermodynamically stable between 200 and 1100 K, but to contain Ti vacancies below this temperature range and N vacancies above $T = 1100$ K, leading to overstoichiometric and understoichiometric TiN_x , respectively. Similarly, ZrN and HfN are expected to be stoichiometric for 500–1400 K and 1200–1400 K, respectively, but to exhibit cation and anion vacancies below and above these temperature ranges, respectively. This is illustrated in Fig. 5 with the white region labeled “Stoichiometric Compounds”, as well as red and green areas which indicate the temperature range for where cation or nitrogen vacancies are stable, respectively. Experimental studies of group 4 nitrides report, consistent with our results, stoichiometric and both over- and understoichiometric compositions, depending on deposition parameters [34,37,41,55]. More specifically, TiN_x with $x < 1$ is grown at growth temperatures of ~ 1000 K and contains nitrogen vacancies at nitrogen partial pressures of 0.07 Pa [34,41,95]. However, increasing the growth pressures to 2.67 Pa results in stoichiometric TiN consistent with our predictions of a stoichiometric TiN in the temperature range of 200–1100 K. This is also in agreement with our predictions that increasing the partial pressure of nitrogen renders nitrogen deficient defects (such as nitrogen vacancies, cation antisites and cation interstitials) energetically less favorable. Similarly, HfN_x has been grown over a large composition range $x = 0.8$ – 1.6 by varying the temperature and the N_2 partial pressure [39,40,42,96]. More specifically, HfN_x deposited at a relatively low temperature $T = 473$ K and a low N_2 partial pressure $p_{\text{N}_2} = 0.03$ Pa is understoichiometric ($x < 1$), but becomes stoichiometric and then over-stoichiometric ($x > 1$) with an increasing nitrogen partial pressure [42], consistent with our predictions of a decreasing favorability of nitrogen deficient defects with increasing pressure. Other experimental studies have reported a similar increase in the nitrogen-to-Hf ratio for HfN_x grown at 923 K, with x increasing from 0.8 for $p_{\text{N}_2} = 0.1$ Pa [39] to $x = 1.5$ for $p_{\text{N}_2} = 2.67$ Pa [39,96]. We note that these results are in perfect qualitative agreement with our predictions, but that our predicted temperature window for growth of stoichiometric HfN, 1200–1400 K, is higher than these experimental studies suggest. We attribute this discrepancy to kinetic factors. More specifically, cation vacancies are predicted to be thermodynamically stable at low temperatures, such that HfN_x growth should lead to nitrogen-rich ($x > 1$) compositions. However, a low temperature may kinetically limit dissociation of N_2 molecules and incorporation of N into the growing layer, such that the composition becomes nitrogen-deficient ($x < 1$), exactly as reported from experiments, particularly at low p_{N_2} .

Group 5 nitrides exhibit similar overall trends as group 4 and 3 nitrides. Cation vacancies are the most stable point defect for over-stoichiometric VN, NbN, TaN, with negative formation energies of -0.7 , -2.1 , and -3.4 eV, respectively. These values are considerably lower than the formation energy of the competing nitrogen interstitial and nitrogen antisite defects, with averages of 1.1 and 6.4 eV, respectively. Similarly, the most stable point defect for under-stoichiometric compositions is the nitrogen vacancy, with $E_f = 0.9$, 0.9, and 0.0 eV for VN, NbN, TaN, while the cation interstitials and cation antisites have average formation energies of 7.5 and 11.9 eV, respectively, and are therefore not expected to form at realistic temperatures.

VN exhibits a relatively narrow temperature range around 400 K over which a stoichiometric composition is expected, while lower and higher temperatures lead to over- and understoichiometry, respectively, similar to the group 4 nitrides. This is in good agreement with experimental observations which report vanadium vacancies at growth temperatures < 703 K (430°C) and nitrogen vacancies at $T > 823$ K for growth with $p_{\text{N}_2} = 2.6$ Pa (20 mTorr) [91], and a narrow temperature region of 703–823 K where VN is grown

stoichiometrically [22,80,91]. We note that our calculations suggest a 200 K critical temperature for the formation of 1% of Schottky defects, as indicated by the blue open symbol in Fig. 5. Thus, stoichiometric VN is expected to simultaneously contain some vacancies of both types. NbN and TaN exhibit at least one stable vacancy defect for any given temperature, consistent with the negative E_f for Schottky defects at all temperatures. More specifically, NbN is expected to contain Nb vacancies < 600 K and N vacancies > 400 K, illustrated by overlapping green and red regions in Fig. 5, while Ta vacancies in TaN are stable < 1500 K and N vacancies are stable at all temperatures. This is in agreement with experimental reports which observe the presence of nitrogen vacancies at 873–1273 K for NbN grown with $p_{\text{N}_2} = 0.67$ Pa [23], as well as niobium vacancies at 300 and 673 K for a relatively low $p_{\text{N}_2} = 0.16$ Pa [28]. In addition, these studies also indicate a trend for over-stoichiometric compositions with increasing p_{N_2} , consistent with our predictions of both niobium and nitrogen vacancies.

In group 6 nitrides, cation vacancies, anion vacancies, cation interstitials, anion interstitials and Schottky pairs are all thermodynamically stable with average formation energies of -2.8 , -1.9 , -4.9 , -9.4 and -4.6 eV, respectively. This is perfectly consistent with the mechanical and thermodynamic instability of group 6 transition metal nitrides in the rock-salt structure [50,51,70,74]. Based on the calculated formation energies, nitrogen and cation interstitials are the most likely defects for over-stoichiometric and under-stoichiometric compositions, respectively. However, all the above-mentioned point defects may be present and will need to be considered when discussing the microstructure of these compounds, which may also relax into ordered lower energy crystal structures. High temperature extrapolation indicates that nitrogen vacancies, nitrogen interstitials and cation interstitials are thermodynamically stable at all temperatures, while cation vacancies remain stable up to 1100 K for CrN, 800 K for MoN and 1200 K for WN. This is in excellent overall agreement with previous reports on MoN and WN which indicate considerable concentrations of both cation and anion vacancies for growth with $p_{\text{N}_2} = 2.67$ Pa and $T = 973$ K [25,26,76].

5. Conclusions

In summary, we have calculated the formation energies of point defects: vacancies, interstitials and antisites in group 3–6 transition metal nitrides with a rocksalt structure. As a general trend, the formation of defects becomes more favorable when moving down the group and to the right in a period. At zero temperature, cation vacancies are thermodynamically stable for group 4–6 nitrides, and nitrogen vacancies for group 6 nitrides. For group 3 nitrides, no point defect is stable, but under- and over-stoichiometric compositions are most likely due to nitrogen vacancies and interstitials, respectively. Antisite defects of both types as well as cation interstitials with the exception of group 6 exhibit relatively high formation energies and are not expected to form in these nitrides. Finite temperature effects are dominated by a decrease in the nitrogen chemical potential due to the entropy of the N_2 vapor phase, while the configurational entropy is an important secondary effect. As a consequence, nitrogen deficient point defects including nitrogen vacancies, cation interstitials, and cation antisites become more favorable with increasing temperature. In contrast, the thermodynamic stability of cation vacancies, nitrogen interstitials, and nitrogen antisites decreases with increasing temperature. A quantitative analysis of these temperature effects leads to predictions of e.g. critical temperatures for the stability of nitrogen vacancies in ScN, YN, and LaN of 1400, 1400, and 900 K; or the temperature ranges for which TiN, ZrN, or HfN are expected to be stoichiometric: 200–1100 K, 500–1400 K, and 1200–1400 K; or the temperature

above which Schottky defects are stable: 200 K for VN and all temperatures for NbN and TaN.

The overall results indicate that thermodynamic considerations can explain a wide range of compositional variations in rocksalt structure transition metal nitrides. More specifically, synthesis in equilibrium with N₂ gas leads to nitrides which are stoichiometric ($x = 1$), over-stoichiometric ($x > 1$) or under-stoichiometric ($x < 1$), depending on pressure, temperature, and metal element. This argument is opposite to the common reasoning (which uses *kinetics* rather than *thermodynamics*) to explain compositional variations and microstructural development of these refractory nitrides during synthesis by reactive sputtering techniques. We do not want to imply that kinetic barriers during deposition can be neglected, since synthesis is typically considered to occur under far-from-equilibrium conditions. However, opposite to current practice, thermodynamic rather than kinetic considerations may explain, to a large extent, the deviations from stoichiometry.

Acknowledgements

The authors acknowledge support by the National Science Foundation under Grant Nos. 1712752, 1629230, 1629239 and 1537984. Computational resources were provided by the Center for Computational Innovations at RPI.

References

- [1] S. Koseki, K. Inoue, S. Morito, T. Ohba, H. Usuki, Comparison of TiN-coated tools using CVD and PVD processes during continuous cutting of Ni-based superalloys, *Surf. Coating. Technol.* 283 (2015) 353–363, <https://doi.org/10.1016/j.surfcoat.2015.10.071>.
- [2] P. Hones, M. Diserens, R. Sanjinés, F. Lévy, Electronic structure and mechanical properties of hard coatings from the chromium–tungsten nitride system, *J. Vac. Sci. Technol. B* 17 (1999) 1024, <https://doi.org/10.1116/1.1320806>.
- [3] J. Musil, Hard and superhard nanocomposite coatings, *Surf. Coating. Technol.* 125 (2000) 322–330, [https://doi.org/10.1016/S0257-8972\(99\)00586-1](https://doi.org/10.1016/S0257-8972(99)00586-1).
- [4] T. Polcar, N.M.G. Parreira, A. Cavaleiro, Structural and tribological characterization of tungsten nitride coatings at elevated temperature, *Wear* 265 (2008) 319–326, <https://doi.org/10.1016/j.wear.2007.10.011>.
- [5] T. Polcar, A. Cavaleiro, Structure, mechanical properties and tribology of W–N and W–O coatings, *Int. J. Refract. Metals Hard Mater.* 28 (2010) 15–22, <https://doi.org/10.1016/j.ijrmhm.2009.07.013>.
- [6] E.C. Samano, a. Clemente, J. a. Díaz, G. Soto, Mechanical properties optimization of tungsten nitride thin films grown by reactive sputtering and laser ablation, *Vacuum* 85 (2010) 69–77, <https://doi.org/10.1016/j.vacuum.2010.04.004>.
- [7] K. Zhang, K. Balasubramanian, B.D. Ozsdolay, C.P. Mulligan, S.V. Khare, W.T. Zheng, D. Gall, Epitaxial NbCxN1-x(001) layers: growth, mechanical properties, and electrical resistivity, *Surf. Coating. Technol.* 277 (2015) 136–143, <https://doi.org/10.1016/j.surfcoat.2015.07.025>.
- [8] H.S. Seo, T.Y. Lee, J.G. Wen, I. Petrov, J.E. Greene, D. Gall, Growth and physical properties of epitaxial HfN layers on MgO(001), *J. Appl. Phys.* 96 (2004) 878–884, <https://doi.org/10.1063/1.1759783>.
- [9] M. Yasuoka, P. Wang, R. Murakami, Comparison of the mechanical performance of cutting tools coated by either a TiCxN1-x single-layer or a TiC/TiC0.5N0.5/TiN multilayer using the hollow cathode discharge ion plating method, *Surf. Coating. Technol.* 206 (2012) 2168–2172, <https://doi.org/10.1016/j.surfcoat.2011.09.053>.
- [10] E.E. Vera, M. Vite, R. Lewis, E.A. Gallardo, J.R. Laguna-Camacho, A study of the wear performance of TiN, CrN and WC/C coatings on different steel substrates, *Wear* 271 (2011) 2116–2124, <https://doi.org/10.1016/j.wear.2010.12.061>.
- [11] Y.L. Su, T.H. Liu, Tribological properties of Ti2N-Wx% coatings deposited by magnetron sputtering, *Vacuum* 77 (2005) 343–354, <https://doi.org/10.1016/j.vacuum.2004.12.004>.
- [12] X. Chen, J. Xu, Q. Xiao, Cutting performance and wear characteristics of Ti(C,N)-based cermet tool in machining hardened steel, *Int. J. Refract. Metals Hard Mater.* 52 (2015) 143–150, <https://doi.org/10.1016/j.ijrmhm.2015.06.006>.
- [13] C. Kral, W. Lengauer, D. Rafaja, P. Ettmayer, Critical review on the elastic properties of transition metal carbides, nitrides and carbonitrides, *J. Alloy. Comp.* 265 (1998) 215–233, [https://doi.org/10.1016/S0925-8388\(97\)00297-1](https://doi.org/10.1016/S0925-8388(97)00297-1).
- [14] L. Hultman, Thermal stability of nitride thin films, *Vacuum* 57 (2000) 1–30, [https://doi.org/10.1016/S0042-207X\(00\)00143-3](https://doi.org/10.1016/S0042-207X(00)00143-3).
- [15] Z.T.Y. Liu, X. Zhou, D. Gall, S.V. Khare, First-principles investigation of the structural, mechanical and electronic properties of the NbO-structured 3d, 4d and 5d transition metal nitrides, *Comput. Mater. Sci.* 84 (2014) 365–373, <https://doi.org/10.1016/j.commatsci.2013.12.038>.
- [16] C.S. Shin, D. Gall, P. Desjardins, A. Vailionis, H. Kim, I. Petrov, J.E. Greene, M. Odén, Growth and physical properties of epitaxial metastable cubic TaN(001), *Appl. Phys. Lett.* 75 (1999) 3808, <https://doi.org/10.1063/1.125463>.
- [17] Z.T.Y. Liu, X. Zhou, S.V. Khare, D. Gall, Structural, mechanical and electronic properties of 3d transition metal nitrides in cubic zincblende, rocksalt and cesium chloride structures: a first-principles investigation, *J. Phys. Condens. Matter* 26 (2014) 25404, <https://doi.org/10.1088/0953-8984/26/2/025404>.
- [18] P. Hones, N. Martin, M. Regula, F. Levy, Structural and mechanical properties of chromium nitride, molybdenum nitride, and tungsten nitride thin films, *J. Phys. D Appl. Phys.* 36 (2003) 1023–1029, <https://doi.org/10.1088/0022-3727/36/8/313>.
- [19] D. Gall, I. Petrov, N. Hellgren, L. Hultman, J.E. Sundgren, J.E. Greene, Growth of poly- and single-crystal ScN on MgO(001): role of low-energy N2+ irradiation in determining texture, microstructure evolution, and mechanical properties, *J. Appl. Phys.* 84 (1998) 6034–6041, <https://doi.org/10.1063/1.368913>.
- [20] J.-E. Sundgren, Structure and properties of TiN coatings, *Thin Solid Films* 128 (1985) 21–44, [https://doi.org/10.1016/0040-6090\(85\)90333-5](https://doi.org/10.1016/0040-6090(85)90333-5).
- [21] A.B. Mei, B.M. Howe, C. Zhang, M. Sardela, J.N. Eckstein, L. Hultman, A. Rockett, I. Petrov, J.E. Greene, Physical properties of epitaxial ZrN/MgO(001) layers grown by reactive magnetron sputtering, *J. Vac. Sci. Technol.* 31 (2013) 61516, <https://doi.org/10.1116/1.4825349>.
- [22] A.B. Mei, R.B. Wilson, D. Li, D.G. Cahill, A. Rockett, J. Birch, L. Hultman, J.E. Greene, I. Petrov, Elastic constants, Poisson ratios, and the elastic anisotropy of VN(001), (011), and (111) epitaxial layers grown by reactive magnetron sputter deposition, *J. Appl. Phys.* 115 (2014) 214908, <https://doi.org/10.1063/1.4881817>.
- [23] K. Zhang, K. Balasubramanian, B.D. Ozsdolay, C.P. Mulligan, S.V. Khare, W.T. Zheng, D. Gall, Growth and physical properties of epitaxial NbN(001) films on MgO(001), *Surf. Coating. Technol.* 288 (2016) 105–114, <https://doi.org/10.1016/j.surfcoat.2016.01.009>.
- [24] D. Gall, C.-S. Shin, T. Spila, M. Odén, M.J.H. Senna, J.E. Greene, I. Petrov, Growth of single-crystal CrN on MgO(001): effects of low-energy ion-irradiation on surface morphological evolution and physical properties, *J. Appl. Phys.* 91 (2002) 3589, <https://doi.org/10.1063/1.1446239>.
- [25] B.D. Ozsdolay, K. Balasubramanian, D. Gall, Cation and anion vacancies in cubic molybdenum nitride, *J. Alloy. Comp.* 705 (2017) 631–637, <https://doi.org/10.1016/j.jallcom.2017.02.072>.
- [26] B.D. Ozsdolay, C.P. Mulligan, K. Balasubramanian, L. Huang, S.V. Khare, D. Gall, Cubic β -WNx layers: growth and properties vs N-to-W ratio, *Surf. Coating. Technol.* 304 (2016) 98–107, <https://doi.org/10.1016/j.surfcoat.2016.06.079>.
- [27] M. Wen, Q.N. Meng, C.Q. Hu, T. An, Y.D. Su, W.X. Yu, W.T. Zheng, Structure and mechanical properties of δ -NbN/SiNx and δ' -NbN/SiNx nano-multilayer films deposited by reactive magnetron sputtering, *Surf. Coating. Technol.* 203 (2009) 1702–1708, <https://doi.org/10.1016/j.jallcom.2009.07.060>.
- [28] M. Benkahoul, E. Martinez, A. Karimi, R. Sanjinés, F. Lévy, Structural and mechanical properties of sputtered cubic and hexagonal NbNx thin films, *Surf. Coating. Technol.* 180–181 (2004) 178–183, <https://doi.org/10.1016/j.surfcoat.2003.10.040>.
- [29] A.Y. Ganin, L. Kienle, G.V. Vajenine, Synthesis and characterisation of hexagonal molybdenum nitrides, *J. Solid State Chem.* 179 (2006) 2339–2348, <https://doi.org/10.1016/j.jssc.2006.05.025>.
- [30] X. Zhao, K.J. Range, High pressure synthesis of molybdenum nitride Mon, *J. Alloy. Comp.* 296 (2000) 72–74, [https://doi.org/10.1016/S0925-8388\(99\)00496-X](https://doi.org/10.1016/S0925-8388(99)00496-X).
- [31] C.L. Bull, P.F. McMillan, E. Soignard, K. Leinenweber, Determination of the crystal structure of δ -Mon by neutron diffraction, *J. Solid State Chem.* 177 (2004) 1488–1492, <https://doi.org/10.1016/j.jssc.2003.11.033>.
- [32] M.R. Hantehzadeh, S.H. Mortazavi, S. Faryadras, M. Ghoranneviss, The effect of temperature on the structure of tantalum nitride (TaN) thin films deposited by DC plasma, *J. Fusion Energy* 31 (2012) 84–88, <https://doi.org/10.1007/s10894-011-9431-2>.
- [33] S. Wang, X. Yu, Z. Lin, R. Zhang, D. He, J. Qin, J. Zhu, J. Han, L. Wang, H. Mao, J. Zhang, Y. Zhao, Synthesis, crystal structure, and elastic properties of novel tungsten nitrides, *Chem. Mater.* 24 (2012) 3023–3028, <https://doi.org/10.1021/cm301516w>.
- [34] C.S. Shin, D. Gall, N. Hellgren, J. Patscheider, I. Petrov, J.E. Greene, Vacancy hardening in single-crystal TiNx(001) layers, *J. Appl. Phys.* 93 (2003) 6025–6028, <https://doi.org/10.1063/1.1568521>.
- [35] C.S. Shin, S. Rudenja, D. Gall, N. Hellgren, T.Y. Lee, I. Petrov, J.E. Greene, Growth, surface morphology, and electrical resistivity of fully strained substoichiometric epitaxial TiNx (0.67 \leq x < 1.0) layers on MgO(001), *J. Appl. Phys.* 95 (2004) 356–362, <https://doi.org/10.1063/1.1629155>.
- [36] T. Lee, K. Ohmori, C.S. Shin, D.G. Cahill, I. Petrov, J.E. Greene, Elastic constants of single-crystal Ti Nx (001) (0.67 \leq x \leq 1.0) determined as a function of x by picosecond ultrasonic measurements, *Phys. Rev. B* 71 (2005) 144106, <https://doi.org/10.1103/PhysRevB.71.144106>.
- [37] G.B. Smith, P.D. Swift, A. Bendavid, TiN x films with metallic behavior at high N/Ti ratios for better solar control windows, *Appl. Phys. Lett.* 75 (1999) 630–632, <https://doi.org/10.1063/1.124463>.
- [38] T.J. Bendavid, A. P.J. Martin, R.P. Netterfield, Kinder, Characterization of the optical properties and composition of TiN, thin films by spectroscopic, *Surf. Interface Anal.* 24 (1996) 627–633, [https://doi.org/10.1002/\(SICI\)1096-9918\(19960916\)24:9<627::AID-SIA149>3.0.CO;2-R](https://doi.org/10.1002/(SICI)1096-9918(19960916)24:9<627::AID-SIA149>3.0.CO;2-R).
- [39] H.S. Seo, T.Y. Lee, I. Petrov, J.E. Greene, D. Gall, Epitaxial and polycrystalline Hf

- Nx ($0.8 \leq x \leq 1.5$) layers on MgO(001): film growth and physical properties, *J. Appl. Phys.* 97 (2005) 83521, <https://doi.org/10.1063/1.1870097>.
- [40] A.J. Perry, On the existence of point defects in physical vapor deposited films of TiN, ZrN, and HfN, *J. Vac. Sci. Technol.* 6 (1988) 2140, <https://doi.org/10.1116/1.575205>.
- [41] M. Stoehr, C.S. Shin, I. Petrov, J.E. Greene, Raman scattering from TiNx ($0.67 \leq x \leq 1.00$) single crystals grown on MgO(001), *J. Appl. Phys.* 110 (2011) 83503, <https://doi.org/10.1063/1.3651381>.
- [42] Z. Gu, C. Hu, X. Fan, L. Xu, M. Wen, Q. Meng, L. Zhao, X. Zheng, W. Zheng, On the nature of point defect and its effect on electronic structure of rocksalt hafnium nitride films, *Acta Mater.* 81 (2014) 315–325, <https://doi.org/10.1016/j.actamat.2014.08.040>.
- [43] R. Lamni, E. Martinez, S.G. Springer, R. Sanjines, P.E. Schmid, F. Levy, Optical and electronic properties of magnetron sputtered ZrNx thin films, *Thin Solid Films* 447–448 (2004) 316–321, <https://doi.org/10.1016/S0040-6090>.
- [44] Z. Zhang, H. Li, R. Daniel, C. Mitterer, G. Dehm, Insights into the atomic and electronic structure triggered by ordered nitrogen vacancies in CrN, *Phys. Rev. B* 87 (2013), <https://doi.org/10.1103/PhysRevB.87.014104>, 014104.
- [45] C.S. Shin, D. Gall, Y.W. Kim, P. Desjardins, I. Petrov, J.E. Greene, M. Odén, L. Hultman, Epitaxial NaCl structure δ -TaNx(001): electronic transport properties, elastic modulus, and hardness versus N/Ta ratio, *J. Appl. Phys.* 90 (2001) 2879–2885, <https://doi.org/10.1063/1.1391214>.
- [46] R. Deng, B.D. Ozsdolay, P.Y. Zheng, S.V. Khare, D. Gall, Optical and transport measurement and first-principles determination of the ScN band gap, *Phys. Rev. B* 91 (2015), 045104, <https://doi.org/10.1103/PhysRevB.91.045104>.
- [47] S. Kerdsonpanya, B. Alling, P. Eklund, Effect of point defects on the electronic density of states of ScN studied by first-principles calculations and implications for thermoelectric properties, *Phys. Rev. B* 86 (2012) 195140, <https://doi.org/10.1103/PhysRevB.86.195140>.
- [48] S.H. Jhi, S.G. Louie, M.L. Cohen, J. Ihm, Vacancy hardening and softening in transition metal carbides and nitrides, *Phys. Rev. Lett.* 86 (2001) 3348–3351, <https://doi.org/10.1103/PhysRevLett.86.3348>.
- [49] C. Hu, X. Zhang, Z. Gu, H. Huang, S. Zhang, X. Fan, W. Zhang, Q. Wei, W. Zheng, Negative effect of vacancies on cubic symmetry, hardness and conductivity in hafnium nitride films, *Scripta Mater.* 108 (2015) 141–146, <https://doi.org/10.1016/j.scriptamat.2015.07.002>.
- [50] K. Balasubramanian, S.V. Khare, D. Gall, Vacancy-induced mechanical stabilization of cubic tungsten nitride, *Phys. Rev. B* 94 (2016) 174111, <https://doi.org/10.1103/PhysRevB.94.174111>.
- [51] K. Balasubramanian, L. Huang, D. Gall, Phase stability and mechanical properties of Mo $_{1-x}$ N $_x$ with $0 \leq x \leq 1$, *J. Appl. Phys.* 122 (2017) 195101, <https://doi.org/10.1103/PhysRevB.94.174111>.
- [52] H. Euchner, P.H. Mayrhofer, H. Riedl, F.F. Klimashin, A. Limbeck, P. Polcik, S. Kolozsvári, Solid solution hardening of vacancy stabilized Ti x W 1-x B 2, *Acta Mater.* 101 (2015) 55–61, <https://doi.org/10.1016/j.actamat.2015.08.048>.
- [53] H. Euchner, P.H. Mayrhofer, Vacancy-dependent stability of cubic and wurtzite Ti 1-x Al x N, *Surf. Coating. Technol.* 275 (2015) 214–218, <https://doi.org/10.1016/j.surfcoat.2015.05.017>.
- [54] F.F. Klimashin, H. Euchner, P.H. Mayrhofer, Computational and experimental studies on structure and mechanical properties of Mo–Al–N, *Acta Mater.* 107 (2016) 273–278, <https://doi.org/10.1016/j.actamat.2016.01.063>.
- [55] G.B. Smith, P.D. Swift, A. Bendavid, G.B. Smith, P.D. Swift, Films with metallic behavior at high N/Ti ratios for better solar control windows TiN x films with metallic behavior at high N/Ti ratios for better solar control windows, *Appl. Phys. Lett.* 630 (1999) 1–4, <https://doi.org/10.1063/1.124463>.
- [56] C.S. Shin, Y.W. Kim, D. Gall, J.E. Greene, I. Petrov, Phase composition and microstructure of polycrystalline and epitaxial TaNx layers grown on oxidized Si(001) and MgO(001) by reactive magnetron sputter deposition, *Thin Solid Films* 402 (2002) 172–182, [https://doi.org/10.1016/S0040-6090\(01\)01618-2](https://doi.org/10.1016/S0040-6090(01)01618-2).
- [57] X.Y. Zhang, J.S. Chawla, B.M. Howe, D. Gall, Variable-range hopping conduction in epitaxial CrN(001), *Phys. Rev. B* 83 (2011) 165205, <https://doi.org/10.1103/PhysRevB.83.165205>.
- [58] L. Tsetseris, N. Kalfagiannis, S. Logothetidis, S.T. Pantelides, Structure and interaction of point defects in transition-metal nitrides, *Phys. Rev. B* 76 (2007) 224107, <https://doi.org/10.1103/PhysRevB.76.224107>.
- [59] E. Mozafari, B. Alling, P. Steneteg, I.A. Abrikosov, Role of N defects in paramagnetic CrN at finite temperatures from first principles, *Phys. Rev. B* 91 (2015) 094101, <https://doi.org/10.1103/PhysRevB.91.094101>.
- [60] N. Koutná, D. Holec, O. Svoboda, F.F. Klimashin, P.H. Mayrhofer, Point defects stabilize cubic Mo-N and Ta-N, *J. Phys. D Appl. Phys.* 49 (2016) 375303, <https://doi.org/10.1088/0022-3727/49/37/375303>.
- [61] L. Yu, C. Stampfl, D. Marshall, T. Eshrich, V. Narayanan, J.M. Rowell, N. Newman, A.J. Freeman, Mechanism and control of the metal-to-insulator transition in rocksalt tantalum nitride, *Phys. Rev. B* 65 (2002), <https://doi.org/10.1103/PhysRevB.65.245110>, 245110–2451105.
- [62] J.P. Perdew, K. Burke, M. Ernzerhof, Generalized gradient approximation made simple, *Phys. Rev. Lett.* 77 (1996) 3865–3868, <https://doi.org/10.1103/PhysRevLett.77.3865>.
- [63] J. Perdew, J. Chevary, S. Vosko, K. Jackson, M. Pederson, D. Singh, C. Fiolhais, Erratum: atoms, molecules, solids, and surfaces: applications of the generalized gradient approximation for exchange and correlation, *Phys. Rev. B* 48 (1993) 4978, <https://doi.org/10.1103/PhysRevB.48.4978.2>, 4978.
- [64] O.Sackur von, Die universelle Bedeutung des sog. elementaren Wirkungsquantums, *Ann. Phys.* 40 (1913) 67–87, <https://doi.org/10.1002/andp.19133450103>.
- [65] R. Bes, Y. Pison, N. Millard-Pinard, S. Gavarini, M. Freyss, First-principles study of rare gas incorporation in titanium nitride, *Phys. Rev. B* 87 (2013), <https://doi.org/10.1103/PhysRevB.87.024104>, 024104.
- [66] Z. Mei, L. Liang, A.M. Yacout, First-principles study of fission gas incorporation and migration in zirconium nitride, *Comput. Mater. Sci.* 133 (2017) 175–184, <https://doi.org/10.1016/j.commatsci.2017.03.019>.
- [67] L.M. Corliss, N. Elliott, J.M. Hastings, Antiferromagnetic structure of CrN, *Phys. Rev.* 117 (1960) 929–935, <https://doi.org/10.1103/PhysRev.117.929>.
- [68] A. Filippetti, N.A. Hill, Magnetic stress as a driving force of structural Distortions: the case of CrN, *Phys. Rev. Lett.* 85 (2000) 5166, <https://doi.org/10.1103/PhysRevLett.85.5166>.
- [69] A. Filippetti, W.E. Pickett, B.M. Klein, Competition between magnetic and structural transitions in CrN, *Phys. Rev. B* 59 (1999) 7043–7050, <https://doi.org/10.1103/PhysRevB.59.7043>.
- [70] M.J. Mehl, D. Finkenstadt, C. Dane, G.L.W. Hart, S. Curtarolo, Finding the stable structures of N 1 - x W x with an ab initio high-throughput approach, *Phys. Rev. B* 91 (2015) 184110, <https://doi.org/10.1103/PhysRevB.91.184110>.
- [71] S.-H. Jhi, J. Ihm, Electronic structure and structural stability of TiCxN1-x alloys, *Phys. Rev. B* 56 (1997) 13826, <https://doi.org/10.1103/PhysRevB.56.13826>.
- [72] D.G. Sangiovanni, L. Hultman, V. Chirita, Supertoughening in B1 transition metal nitride alloys by increased valence electron concentration, *Acta Mater.* 59 (2011) 2121–2134, <https://doi.org/10.1016/j.actamat.2010.12.013>.
- [73] S.-H. Jhi, J. Ihm, S.G. Louie, M.L. Cohen, Electronic mechanism of hardness enhancement in transition-metal carbonitrides, *Nature* 399 (1999) 132–134, <https://doi.org/10.1038/20148>.
- [74] L. Zhou, F. Kormann, D. Holec, M. Bartosik, B. Grabowski, J. Neugebauer, P.H. Mayrhofer, Structural stability and thermodynamics of CrN magnetic phases from ab initio calculations and experiment, *Phys. Rev. B* 90 (2014) 184102, <https://doi.org/10.1103/PhysRevB.90.184102>.
- [75] K. Balasubramanian, S.V. Khare, D. Gall, Valence electron concentration as an indicator for mechanical properties in rocksalt structure nitrides, carbides and carbonitrides, *Acta Mater.* 152 (2018) 175–185, <https://doi.org/10.1016/j.actamat.2018.04.033>.
- [76] B.D. Ozsdolay, C.P. Mulligan, M. Guerette, L. Huang, D. Gall, Epitaxial growth and properties of cubic WN on MgO(001), MgO(111), and Al₂O₃(0001), *Thin Solid Films* 590 (2015) 276–283, <https://doi.org/10.1016/j.tsf.2015.08.002>.
- [77] N. Terao, Structure of tantalum nitrides, *Jpn. J. Appl. Phys.* 10 (1971) 248–259, <https://doi.org/10.1143/JJAP.10.248>.
- [78] C.R. Weinberger, X.X. Yu, H. Yu, G.B. Thompson, Ab initio investigations of the phase stability in group IVB and VB transition metal nitrides, *Comput. Mater. Sci.* 138 (2017) 333–345, <https://doi.org/10.1016/j.commatsci.2017.07.005>.
- [79] E.I. Isaev, S.I. Simak, I.A. Abrikosov, R. Ahuja, Y.K. Vekilov, M.I. Katsnelson, A.I. Lichtenstein, B. Johansson, Phonon related properties of transition metals, their carbides, and nitrides: a first-principles study, *J. Appl. Phys.* 101 (2007) 123519, <https://doi.org/10.1063/1.2747230>.
- [80] A.B. Mei, O. Hellman, N. Wireklint, C.M. Schlepütz, D.G. Sangiovanni, B. Alling, A. Rockett, L. Hultman, I. Petrov, J.E. Greene, Dynamic and structural stability of cubic vanadium nitride, *Phys. Rev. B* 91 (2015) 054101, <https://doi.org/10.1103/PhysRevB.91.054101>.
- [81] V.I. Ivashchenko, P.E.A. Turchi, E.I. Olifan, Phase stability and mechanical properties of niobium nitrides, *Phys. Rev. B* 82 (2010) 054109, <https://doi.org/10.1016/j.jijhydene.2014.09.033>.
- [82] B.D. Ozsdolay, X. Shen, K. Balasubramanian, G. Scannell, L. Huang, M. Yamaguchi, D. Gall, Elastic constants of epitaxial cubic MoNx(001) layers, *Surf. Coating. Technol.* 325 (2017) 572, <https://doi.org/10.1016/j.surfcoat.2017.07.015>.
- [83] D. Gall, M. Stoehr, J.E. Greene, Vibrational modes in epitaxial Ti 1-x Sc x N (001) layers: an ab initio calculation and Raman spectroscopy study, *Phys. Rev. B* 64 (2001) 174302, <https://doi.org/10.1103/PhysRevB.64.174302>.
- [84] B. Saha, J. Acharya, T.D. Sands, U.V. Waghmare, Electronic structure, phonons, and thermal properties of ScN, ZrN, and HfN: a first-principles study, *J. Appl. Phys.* 107 (2010) 33715, <https://doi.org/10.1063/1.3291117>.
- [85] N. Shulumba, B. Alling, O. Hellman, E. Mozafari, P. Steneteg, M. Odén, I.A. Abrikosov, Vibrational free energy and phase stability of paramagnetic and antiferromagnetic CrN from ab initio molecular dynamics, *Phys. Rev. B* 89 (2014) 174108, <https://doi.org/10.1103/PhysRevB.89.174108>.
- [86] P. Atkins, J. De Paula, *Physical Chemistry*, W.H. Freeman, 2010.
- [87] A.F. Young, C. Sanloup, E. Gregoryanz, S. Scandolo, R.J. Hemley, H.K. Mao, Synthesis of novel transition metal nitrides IrN₂ and OsN₂, *Phys. Rev. Lett.* 96 (2006) 155501, <https://doi.org/10.1103/PhysRevLett.96.155501>.
- [88] A. Friedrich, B. Winkler, L. Bayarjargal, W. Morgenroth, E.A. Juarez-Arellano, V. Milman, K. Refson, M. Kunz, K. Chen, Novel rhenium nitrides, *Phys. Rev. Lett.* 105 (2010), <https://doi.org/10.1103/PhysRevLett.105.085504>, 085504.
- [89] A. Zerr, G. Miehe, J. Li, D.A. Dzyvenko, V.K. Bulatov, H. Höfer, N. Boifan-Casanova, M. Fialin, G. Brey, T. Watanabe, M. Yoshimura, High-pressure synthesis of tantalum nitride having orthorhombic U 253 structure, *Adv. Funct. Mater.* 19 (2009) 2282–2288, <https://doi.org/10.1002/adfm.200801923>.
- [90] S.M. Wang, X.H. Yu, Z.J. Lin, R.F. Zhang, D.W. He, J.Q. Qin, J.L. Zhu, J. Han, L. Wang, H.K. Mao, J.Z. Zhang, Y.S. Zhao, Synthesis, crystal structure, and elastic properties of novel tungsten nitrides, *Chem. Mater.* 24 (2012) 3023–3028, <https://doi.org/10.1021/cm301516w>.
- [91] A.B. Mei, M. Tuteja, D.G. Sangiovanni, R.T. Haasch, A. Rockett, L. Hultman, I. Petrov, J.E. Greene, Growth, nanostructure, and optical properties of epitaxial VN x/MgO(001) ($0.80 \leq x \leq 1.00$) layers deposited by reactive magnetron sputtering, *J. Mater. Chem. C* 4 (2016) 10–12, <https://doi.org/>

- 10.1039/C6TC02289H.
- [92] L. Porte, Stoichiometric scN and nitrogen deficient scandium nitride layers studied by photoelectron spectroscopy, *J. Phys. C Solid State Phys.* 18 (1985) 6701–6709, <https://doi.org/10.1088/0022-3719/18/36/024>.
- [93] R. Niewa, D.A. Zherebtsov, M. Kirchner, M. Schmidt, W. Schnelle, New ways to high-quality bulk scandium nitride, *Chem. Mater.* 16 (2004) 5445–5451, <https://doi.org/10.1021/cm048667y>.
- [94] H. Al-brithen, E.M. Trifan, D.C. Ingram, A.R. Smith, D. Gall, Phase stability, nitrogen vacancies, growth mode, and surface structure of ScN(001) under Sc-rich conditions, *J. Cryst. Growth* 242 (2002) 345–354, [https://doi.org/10.1016/S0022-0248\(02\)01447-1](https://doi.org/10.1016/S0022-0248(02)01447-1).
- [95] M.A. Wall, D.G. Cahill, I. Petrov, D. Gall, J.E. Greene, Nucleation kinetics versus nitrogen partial pressure during homoepitaxial growth of stoichiometric TiN(001): a scanning tunneling microscopy study, *Surf. Sci.* 581 (2005) L122–L127, <https://doi.org/10.1016/j.susc.2005.03.007>.
- [96] H.S. Seo, T.Y. Lee, J.G. Wen, I. Petrov, J.E. Greene, D. Gall, Growth and physical properties of epitaxial HfN layers on MgO(001), *J. Appl. Phys.* 96 (2004) 878–884, <https://doi.org/10.1063/1.1759783>.